JOURNAL OF GEOPHYSICAL RESEARCH, VOL. 93, NO. B6, PAGES 6077–6089, JUNE 10, 1988

Hydrothermal Brecciation in the Jemez Fault Zone, Valles Caldera, New Mexico: Results From Continental Scientific Drilling Program Core Hole VC-1

JEFFREY B. HULEN AND DENNIS L. NIELSON

University of Utah Research Institute, Salt Lake City

An unusual breccia sequence penetrated in the lower 30 m of Continental Scientific Drilling Program core hole VC-1 (total depth 856 m) records a complex hydrothermal history culminating in hydraulic rock rupture and associated alteration at the edge of the Quaternary Valles caldera. The breccias, both tectonic and hydrothermal in origin, were formed in the Jemez fault zone, near the intersection of this major regional structure with the caldera's ring-fracture margin. Tectonic breccias in the sequence are contorted, crushed, and sheared. Coexisting hydrothermal breccias lack such frictional textures but display matrix flow foliation and prominent clast rounding, features characteristic of fluidization. These hydrothermal breccias were intensely altered, during at least five major stages, to quartz-illite-phengite-pyrite aggregates; traces of molybdenite occur locally. This assemblage indicates interaction with hydrothermal fluid at temperatures in excess of 200°C. The extrapolated present maximum temperature of 184°C in the breccia zone therefore represents considerable cooling since these phases were formed. Fluid inclusions in the breccias also preserve evidence of the prior passage of hotter fluids. The inclusions are principally two phase, liquid rich, secondary in origin, and concentrated in hydrothermal quartz. Older, high-salinity inclusions, unrelated to brecciation, homogenize in the temperature range 189°–246°C. Younger inclusions, in part of interbreccia origin, are low-salinity and homogenize in the temperature range 230°–283°C; locally coexisting liquid- and vapor-rich inclusions document periodic boiling of the dilute fluids. These fluid-inclusion data, along with the probable age of the hydrothermal breccias (< 1.5 Ma), the assumed depth at which they developed (about 515 m), and the contemporaneous state of stress (extensional) can be combined to model hydrothermal brecciation at the VC-1 site. The minimum fluid pressure (P_{fr}) required to hydrofracture these rocks was probably about 7.5 MPa (0.0146 MPa/m). A boiling point versus depth curve based on these P_{fr} values graphically defines the physical conditions prevailing when the breccias were formed. When fluid pressure at the assumed depth of brecciation exceeded that curve, in response to rapid release of confining pressure possibly augmented by renewed heating, flashing hydrothermal fluid fractured the enclosing rock. Large overpressures, most likely induced by sudden seismic cracking of a hydrothermally sealed portion of the Jemez fault zone, led to local fluidization of the resulting breccias. Late quartz veining, hydrothermal alteration, and molybdenite mineralization were probably produced by the fluids responsible for brecciation.

INTRODUCTION

Hydrothermal breccias are common features of active, high-temperature geothermal systems and their fossil equivalents, epithermal ore deposits. These breccias and associated hydraulic fracture networks not only focus thermal fluid flow [*Grindley and Browne*, 1976], but are also important ore hosts [*Phillips*, 1972; *Sillitoe*, 1985]. In the active Waiotapu system, New Zealand [*Hedenquist and Henley*, 1985], for example, ore-grade precious-metal precipitates are presently forming in hot spring pools occupying phreatic explosion craters, the surface expressions of deeper hydrothermal brecciation. Hydraulic breccias and stockworks are also the principal ore hosts in hot spring type gold orebodies [*Berger*, 1985; *Lehrman*, 1987] and are frequently encountered in deeper epithermal deposits [*Fournier*, 1983]. Both geothermal and precious-metal exploration and development therefore should benefit from a clearer understanding of the physical processes governing hydraulic rock rupture.

Hydrothermal breccias penetrated near the bottom of Continental Scientific Drilling Program (CSDP) core hole VC-1, just southwest of the Valles caldera complex in north central New Mexico (Figure 1), provide an excellent opportunity to characterize hydraulic rock rupture in a long-active, caldera-hosted, high-temperature geothermal system. Although this system has been extensively explored by a series of deep, rotary geothermal wells [*Union Oil Company of California*, 1982], the cuttings recovered from these wells provide only scant textural information about the faults, fractures, and probable breccias intersected at depth. Detailed study of continuous core from the hydrothermally brecciated rocks of VC-1 therefore also contributes to our knowledge of critical structural controls on intracaldera thermal fluid flow.

The VC-1 hydrothermal breccias host abundant fluid inclusions, many of which were trapped during brecciation. Homogenization temperatures and corresponding freezing-point depressions for these inclusions, when combined with alteration mineralogy and paragenesis as well as the inferred geologic history at the VC-1 site, allow development of a model of hydrothermal brecciation which should be broadly applicable in similar settings worldwide.

METHODS AND PROCEDURES

Characterization of the deep VC-1 breccias began with detailed lithologic logging of core from the lower 50 m of the core hole and progressed through petrographic examination, X ray diffraction (XRD) analysis, and fluid-inclusion studies. Samples selected for XRD, nominally at 1.5-m intervals, were prepared for bulk analysis by light crushing, then hand grinding a representative 1-g split in acetone to < 325 mesh (< 42 μm). These finely ground samples were irradiated at 2°2θ from

Paper number 7B7051.
0148-0227/88/007B-7051$05.00

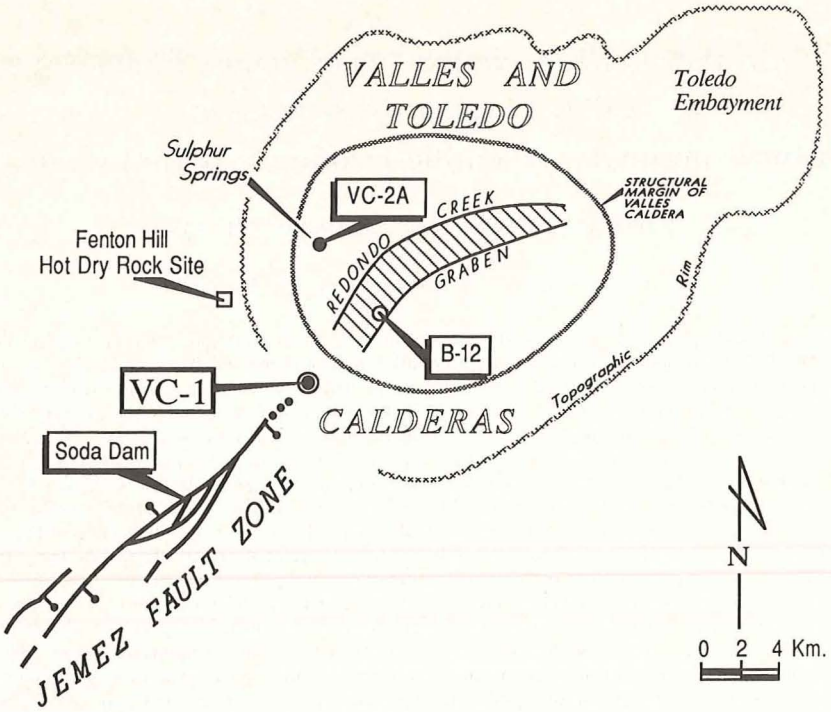

Fig. 1. Location map, showing position of CSDP core hole VC-1 relative to the Valles caldera complex and the Jemez fault zone in north central New Mexico.

2° to 65°2θ using a Phillips diffractometer with CuKα radiation source, theta compensating slit, 0.2-mm (1/2°) receiving slit, and focusing monochromator. Instrument settings were as follows: accelerating voltage 40 kV, tube current 40 mA, time constant 1/2 s, full-scale deflection 2500 c/s, and chart speed 25.4 mm/min. Approximate weight percentages of minerals identified on corresponding diffractograms were determined by comparing diagnostic peak intensities with those of standard phases, with appropriate corrections for matrix absorption. Clay fractions (<5 μm for this study) were extracted from the lightly crushed bulk samples by acoustic disaggregation in deionized water, Stokes' law settling, and centrifugation. The resulting slurries were smeared on glass slides and irradiated at 1°2θ per minute after each of the following treatments: air drying (2°–37°2θ), vapor glycolation at 60°C for 24 hours (2°–22°2θ), heating at 250°C for 1 hour (2°–15°2θ), and heating at 550°C for 1 hour (2°–15°2θ). Instrument settings were the same as for the bulk scans except for the time constant, maintained at 1 s. Approximate percentages of layer silicates identified on diffractograms corresponding to the above treatments were determined by reference to calibration curves (diagnostic peak intensity versus weight percent) previously prepared using standard phases mixed in various proportions.

Whenever possible, the expandable interlayer content of illite and mixed-layer illite/smectite in the VC-1 clay fractions was determined using the methods of *Środoń* [1980]. The less accurate, but more generally applicable techniques of *Reynolds* [1980] were used to calculate this value when peak overlap due to contamination by nonclay phases precluded use of the Środoń method. On selected test samples, expandable interlayer contents determined by both methods were separated by no more than 10%.

Samples for fluid-inclusion analysis were prepared by doubly polishing rock chips 200–400 μm in thickness and 5–10 mm in diameter. Homogenization temperatures and freezing-point depressions of fluid inclusions in these chips were measured using a Fluid Inc. modified USGS gas-flow heating/freezing system. Slow heating rates (0.5°C/min or less) and careful calibration ensured optimum accuracy and reproducibility ($\pm$ 0.2°C).

Geologic Setting

Core hole VC-1 is located immediately southwest of the Valles caldera complex (Figure 1), comprising the 1.12-Ma Valles caldera [*Self et al.*, 1986], its spatially coincident predecessor, the 1.45-Ma Toledo caldera [*Self et al.*, 1986; *Heiken et al.*, 1986], and possibly small precursor calderas formed at the same site between 3.6 and 1.45 Ma [*Nielson and Hulen*, 1984; *Self et al.*, 1986]. Calderas of the Valles complex represent the culminating volcanic episode in the Jemez volcanic field, active since at least 16 Ma [*Gardner et al.*, 1986]. This volcanic field appears to have been localized by the intersection of western boundary faults of the Rio Grande Rift with the Jemez lineament, a northeast trending regional feature defined by alignment of Cenozoic volcanic centers and major structures such as the Jemez fault zone (Figure 1) [*Laughlin*, 1981].

Evolution of the Valles caldera complex was probably under way by 3.6 Ma, when low-volume, felsic ash flow tuffs began erupting near the center of the Jemez volcanic field [*Self et al.*, 1986]. Expulsion of these tuffs probably led to development of a small caldera or set of calderas now completely concealed by Valles caldera fill [*Nielson and Hulen*, 1984; *Self et al.*, 1986]. Felsic ignimbrites aggregating approximately 300 km^3 were violently ejected at 1.45 Ma, resulting in emplacement of the Otowi Member of the Bandelier Tuff and formation of the Toledo caldera [*Doell et al.*, 1968; *Izett et al.*, 1980; *Self et al.*, 1986]. At 1.12 Ma, a second major felsic pyroclastic eruption of roughly equivalent volume produced the Tshirege Member of the Bandelier Tuff [*Izett et al.*, 1980; *Self et al.*, 1986]. The Tshirege eruption destroyed most of the Toledo caldera but resulted in formation of the Valles caldera at essentially the same site [*Heiken et al.*, 1986]. Collapse of the Valles caldera was followed shortly by resurgent doming.

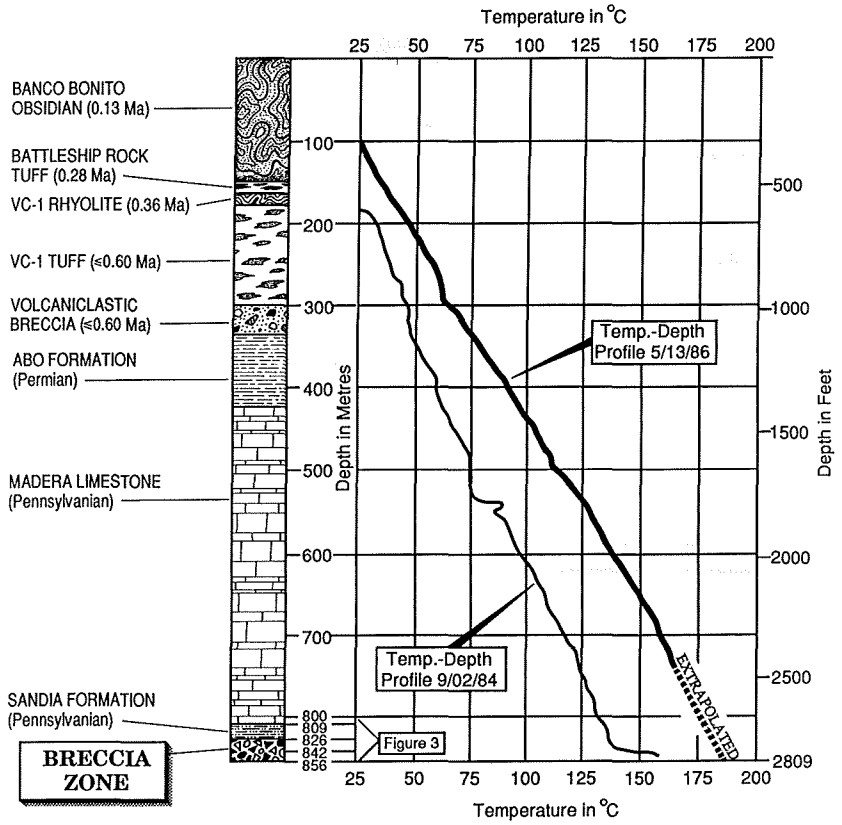

Fig. 2. Generalized stratigraphic and temperature log for core hole VC-1. Tectonic and hydrothermal breccia interval discussed in this paper spans the depth range 826–856 m. Modified from *Goff et al.* [1986]. Ages of individual volcanic units from *Gardner et al.* [1986] and F. Goff and J. Gardner (personal communication, 1987).

The apical graben of the resurgent Redondo dome and the ring-fracture zone of the Valles caldera ("structural margin" on Figure 1) subsequently guided emplacement of rhyolite domes and flows until about 0.13 Ma [*Gardner et al.*, 1986].

VC-1 is collared just southwest of the intersection of the Valles caldera's structural margin with the subsurface projection of the Jemez fault zone (Figure 1). A major crustal flaw since perhaps Pennsylvanian time (J. N. Gardner, personal communication, 1986), the Jemez fault zone not only controls the location of the apical graben of the Valles caldera's resurgent dome, it also focuses the southwesterly flowing hydrothermal plume draining the caldera's active geothermal systems [*Goff et al.*, 1986]. Since late Miocene, the Jemez fault zone has been characterized by exclusively normal displacement; prior strike-slip movement, however, is locally evident [*Aldrich and Laughlin*, 1984].

The active high-temperature hydrothermal system of the Valles caldera was explored by Union Oil Company (UOC), now Unocal, between 1971 and 1982 [*Union Oil Company*, 1982]. UOC concentrated its exploration efforts on the two areas of highest heat flow and most intense surficial alteration in the Valles caldera, the Redondo Creek graben and the Sulphur Springs area, near the western structural margin (Figure 1). Liquid-dominated conditions prevail below a nominal depth of 500 m in both areas. Hydrothermal fluids in this regime are high-temperature (up to about 300°C), neutral-chloride waters ranging from 5000 to 18,000 mg/kg total dissolved solids [*Truesdell and Janik*, 1986; *White*, 1986; *Shevenell et al.*, 1987]; temperatures up to 341°C have been recorded in impermeable rocks beneath the hydrothermal system [*Nielson and Hulen*, 1984].

Circulating in permeable faults, fractures, and breccias as well as discrete sandstone and nonwelded tuff horizons [e.g., *Hulen and Nielson*, 1982], thermal fluids of the Valles caldera have interacted with their host rocks to form distinct alteration assemblages [*Hulen and Nielson*, 1986*a*, *b*; *Hulen et al.*, 1987]. Intense phyllic (and locally potassic) alteration is diagnostic of principal fluid conduits; propylitic alteration prevails away from these channels. Water vapor is now the pressure-controlling fluid to an average depth of about 500 m, but a shallow, widespread cap of mixed layer illite/smectite indicates that the liquid-dominated reservoir once extended up to (and probably above) the present ground surface. This conclusion is corroborated by the occurrence of near-surface molybdenite-quartz-fluorite mineralization in the Sulphur Springs area [*Hulen et al.*, 1987]. Only a veneer of scattered, acid-sulfate advanced argillic alteration, concentrated at Sulphur Springs [*Goff and Gardner*, 1980; *Charles et al.*, 1986] is related to contemporary, shallow, vapor-dominant conditions.

Active geothermal systems of the Valles caldera are clearly analogs of fossil systems responsible for depositing various epithermal ores. *Hulen and Nielson* [1986*a*, *b*] noted numerous parallels between the active Valles systems and those which formed Creede-type, epithermal silver/base metal deposits. *Hulen et al.*, [1987] documented unique, sub-ore grade, epithermal molybdenite mineralization in <1.12-Ma tuffs penetrated in CSDP core hole VC-2A, at Sulphur Springs (Figure 1). This occurrence, along with traces of molybdenite in the VC-1 hydrothermal breccias discussed in this paper, may be the near-surface expression of deeply concealed, Climax- or granite-type molybdenum mineralization.

Figure 2 is a generalized stratigraphic and temperature log for VC-1. To a depth of 333 m, the hole penetrates post-Bandelier rhyolite flows, tuffs, and breccias ranging in age

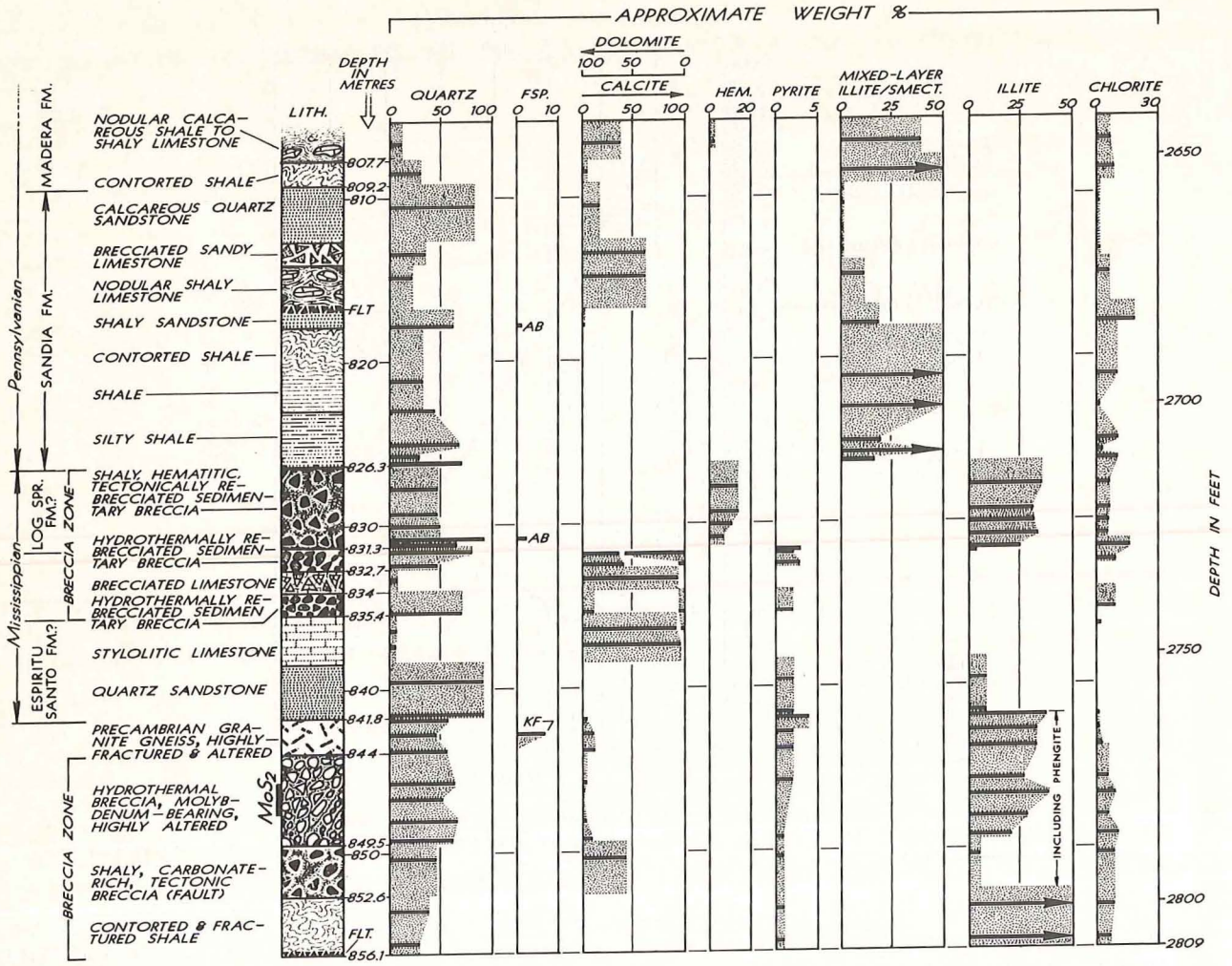

Fig. 3. Detailed lithologic and alteration log of the lower portion of core hole VC-1 (806–856.1 m), showing tectonic and hydrothermal breccia intercepts. Downhole histograms at right display distributions of rock-forming and alteration phases as determined by bulk XRD analysis. Actual values shown by black bars; stippling between bars added only for clarity. AB, albite; FLT, fault; FM, formation; FSP, feldspar; HEM, hematite; KF, potassium feldspar; LITH, lithology; and MoS_2, molybdenite.

between 0.13 and 0.60 Ma [*Gardner et al.*, 1986; J. Gardner and F. Goff, personal communication, 1986]. Beneath this young volcanic sequence, red beds of the Permian Abo Formation extend to a depth of 424 m. Two Pennsylvanian formations were intersected: the Madera Limestone, a dominantly marine carbonate sequence between 424 and 809 m, and the Sandia Formation, a near-shore, calcareous siliciclastic unit extending from the base of the Madera to a depth of 826 m.

This paper focuses on the lower 30 m of VC-1 (826–856 m; Figure 2). This is an extremely complex interval comprising deformed, hydrothermally altered Paleozoic sedimentary rocks and Precambrian gneiss. The intense brecciation of these rocks, together with the location of VC-1 (Figure 1), strongly suggests that the bottom of the core hole penetrates a subsurface extension of the Jemez fault zone.

Maximum measured temperatures in the VC-1 breccia zone do not exceed 161°C, but the latest logs extrapolate to 184°C at total depth (Figure 2). We will present evidence from alteration assemblages and fluid-inclusion microthermometry, however, that fluids circulating in these rocks attained temperatures approaching 300° in the geologically recent past.

Stratigraphy

Much of the VC-1 breccia zone, spanning the depth interval 826.2–856.1 m and detailed in Figure 3, is so thoroughly disrupted and altered that its components cannot be ascribed to particular stratigraphic units. Portions of the zone, however, are sufficiently intact that relict texture and mineralogy can be used for identification. In this section, we will briefly describe these relatively undisturbed rocks and attempt to correlate them with formally designated formations in north central New Mexico, primarily as a framework for discussing the tectonic and hydrothermal breccias they host.

The deepest VC-1 rock unit that can be correlated confidently with a regional counterpart is the Precambrian gneiss intersected between depths of 841.8 and 844 m (Figures 3 and 4). Although highly fractured, quartz sericitized, and cut by numerous hydrothermal veinlets, this rock is still recognizable as a weakly foliated, medium-crystalline, granitic orthogneiss. The rock is texturally identical to the unaltered gneiss penetrated below a depth of 3115 m in UOC borehole B-12, about 5 km to the northeast in the Valles caldera (Figure 1). It is also very similar to gneiss in the nearest Precambrian ex-

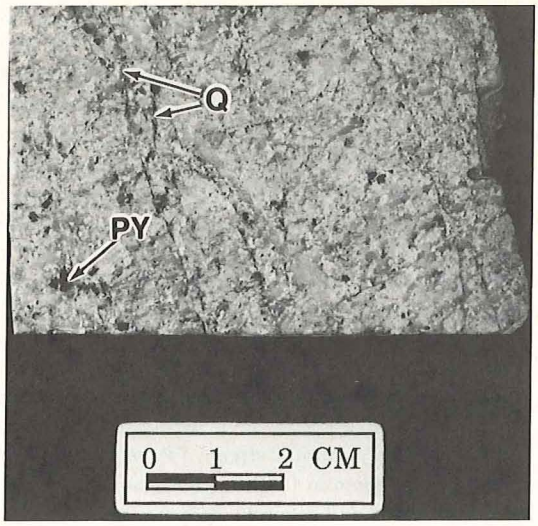

Fig. 4. Quartz-sericitized, intensely fractured, Precambrian granitic orthogneiss from the depth interval 842.8–842.9 m (top to left). Note relict gneissic foliation inclined to the right at 45° to the core axis. Q, quartz veinlet; PY, disseminated pyrite.

posure, near Soda Dam (Figure 1). In thin section, the VC-1 gneiss is seen to be so thoroughly disrupted that it actually consists of rock "islands" separated by thin rock-flour septa or hydrothermal veinlets. Thus it is technically a breccia. However, clasts generally account for greater than 95 vol %, and the parentage of the rock is readily recognizable; therefore it will be referred to simply as gneiss.

The gneiss "islands" noted above consist of polycrystalline quartz aggregates which are commonly granoblastically recrystallized and intergrown with weakly to strongly sericitized microcline and orthoclase as well as stubby lath-shaped sericite aggregates replacing primary plagioclase. "Sericite" in this case and throughout this paper refers to fine-crystalline illite as well as phengite, a gray-green, iron-rich, illite analog. The Precambrian gneiss also contains up to 3% coarse-crystalline (1–2 mm in diameter) mica, principally muscovite with traces of feebly pleochroic light brown biotite. Apatite, zircon, sphene, rutile, and hematite (replacing magnetite or ilmenite) are present in trace amounts.

Resting unconformably on the orthogneiss in VC-1 is a well-bedded, fine- to medium-grained quartz sandstone 3.3 m in thickness (Figure 3). Semiquantitative bulk XRD analysis shows that this sandstone is approximately 92% (weight) quartz, with 2% pyrite and 6% illite; petrographic examination reveals the additional presence of traces of detrital potassium feldspar. Most of the quartz is detrital, but some occurs as a fine-crystalline cement. The illite, principally interstitial, is probably a hydrothermally recrystallized authigenic or diagenetic variety.

The quartz sandstone is overlain by 3.1 m of fine- to coarse-crystalline, stylolitic and locally laminated limestone (Figure 3). Consisting principally of calcite (92–95%), this limestone also contains minor (5%) detrital quartz; traces of illite, chlorite, and pyrite are concentrated in stylolites.

Both the stylolitic limestone and underlying quartz sandstone may represent the Espiritu Santo Formation of the Mississippian Arroyo Peñasco Group [*Armstrong and Mamet*, 1974]. Wherever observed in north central New Mexico, this formation rests unconformably on Precambrian basement rock and consists of a basal clastic horizon (the Del Padre Sandstone Member) and an overlying carbonate sequence.

Clasts in a complexly brecciated and altered interval between depths of 831.3 and 835.4 m, immediately above the stylolitic limestone (Figure 3), are of unknown stratigraphic affiliation. This breccia zone and others deep in VC-1 will be discussed in detail in the following section on tectonic and hydrothermal brecciation.

A distinctive, hematitic, rebrecciated sedimentary breccia spans the depth interval 826.3–831.3 m (Figure 3). This rock, originally a chert-bearing red bed, will also be described in more detail in the following section. The salient primary features of this unit are its brick red, hematitic, argillaceous to sandy matrix and abundant, angular chert clasts (Figure 5). Diagenetic illite and chlorite, locally hydrothermally recrystallized, are the principal matrix constituents.

Assuming that the Precambrian gneiss in VC-1 is overlain by the Mississippian Espiritu Santo Formation, as discussed above, the chert-bearing red bed breccia may represent the overlying Log Springs Formation, of uppermost Mississippian age [*Armstrong and Mamet*, 1974]. At the type locality in the southwestern Nacimiento Mountains, about 30 km southwest of VC-1, the Log Springs Formation consists of hematitic shale, sandstone, and conglomerate. Coarser clastic units contain angular to rounded pebbles of Mississippian chert and limestone as well as Precambrian gneiss and schist. At Guadalupe Box, about 16 km southwest of VC-1, the formation is entirely red ferruginous shale [*DuChene*, 1974]. The iron-rich character and brick red coloration of the Log Springs Formation throughout north central New Mexico are believed to indicate deposition of the unit as a residual soil or regolith [*Armstrong and Mamet*, 1974].

Between depths of 809.2 and 826.3 m, immediately above the presumed Log Springs Formation, VC-1 penetrated a dominantly siliciclastic sequence which is probably the Pennsylvanian Sandia Formation (Figure 3) [*Gordon*, 1907; *Kelley and Northrop*, 1975]. Like the Sandia Formation throughout northern New Mexico, this sequence appears to have been

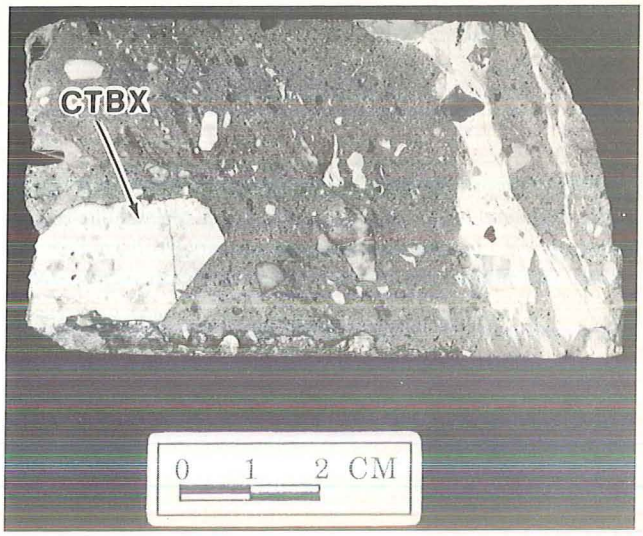

Fig. 5. Shaly, hematitic, tectonically rebrecciated sedimentary breccia from the depth interval 829.6–829.7 m (top to left). Note prominent shearing of matrix. CTBX marks recrystallized, sparsely chloritic chert breccia clast cut by hydrothermal quartz veinlet truncated at clast margins.

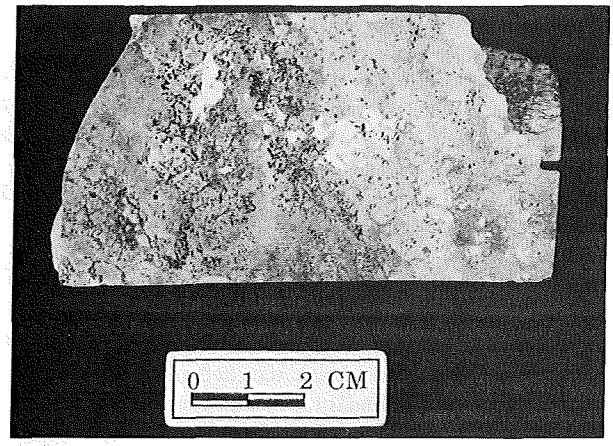

Fig. 6. Portion of a mineralized, dolomitic limestone breccia clast in hydrothermal breccia from the depth interval 831.8–831.9 m (top to left). Breccia texture of the clast partially obscured by recrystallization of carbonates. Dark grains are disseminated, postbreccia, hydrothermal magnetite, pyrite, and rare hematite. White clasts are disrupted, prebreccia hydrothermal barite.

deposited in a rapidly fluctuating marine shoreline environment [*DuChene*, 1974; *Siemers*, 1983; *Baltz and Myers*, 1984]. The upper contact of the Sandia in VC-1 with the overlying Pennsylvanian Madera Limestone is characteristically transitional. The boundary between the two formations in the core hole is arbitrarily placed, as suggested by *Loughlin and Koschmann* [1942], at the top of a prominent sandstone above which limestones are predominant and below which terrigenous strata are more prevalent.

Calcareous quartz sandstone, shaly limestone, and shale are the principal lithologies of the VC-1 Sandia Formation (Figure 3). Layer silicates are locally abundant in these rocks, particularly in shaly horizons. Illite-rich, mixed layer illite/smectite is predominant, but iron-rich chlorite is also common. The illite/smectite is principally of diagenetic origin [see also *Keith*, this issue] but is hydrothermally recrystallized within and adjacent to more permeable zones in the Sandia Formation. Post-Sandia hydrothermal illite/smectite occurs locally as a vein- and vug-filling phase. Chlorite in the Sandia Formation is also of both diagenetic and hydrothermal origin.

TECTONIC AND HYDROTHERMAL BRECCIAS

Introduction

Below a depth of 826.3 m, the Paleozoic and Precambrian rocks discussed above are disrupted into a spectacular breccia sequence (Figure 3) of both tectonic and hydrothermal origin. Before describing each of the major breccias in this sequence, we will briefly discuss the textural evidence for their genesis.

Tectonic breccias are texturally distinct from those formed by hydrothermal processes, although transitional varieties can be difficult to identify with confidence. Textures of tectonic breccias reflect their cataclastic origin; original rocks are brittly fragmented, with rotation of clasts, grain boundary sliding, and granulation [*Sibson*, 1977]; slickensides are commonly present. Hydrothermal breccias, by contrast, lack these frictional textures, displaying instead evidence of an explosive origin.

Two end-member varieties of hydrothermal breccia are common in both active and fossil geothermal systems: "jigsaw puzzle" breccias and those that have undergone fluidization. Jigsaw puzzle breccias, such as those of the Waiotapu geothermal system, New Zealand [*Hedenquist and Henley*, 1985], are created by explosive, hydraulic expansion of a fractured host rock. This expansion may be accompanied by forceful ejection of fragments from the walls into the interiors of open fissures [e.g., *Grindley and Browne*, 1976]. Fragments in these breccias are typically subangular to angular, show minimal rotation, and are only slightly displaced from their points of origin. The matrix, comprising smaller fragments, rock flour, and hydrothermal phases in various proportions, shows no evidence of crushing or shearing unless modified by subsequent tectonic activity.

Textures of fluidized breccias provide evidence of their formation in a more energetic hydrothermal regime. Fluidization involves suspension, abrasion, and sometimes entrainment and transport of rock fragments in a highly overpressured, outward escaping gas or liquid stream [*Reynolds*, 1954; *McCallum*, 1985]. Fragments in fluidized breccias, depending on the degree of transport and attrition, may be angular to extremely well rounded. The matrix is commonly flow foliated, with both lamellar and turbulent foliation locally present. Neither matrix nor clasts, however, unlike their counterparts in tectonic breccias, are crushed, sheared, or disrupted by slickensides.

Breccias of VC-1

Tectonic and hydrothermal breccias below a depth of 826.3 m in VC-1 almost certainly formed in a branch of the Jemez fault zone (Figure 1). The core hole is collared directly above the subsurface northeastern extension of this structure, and major tectonic displacement of the VC-1 rocks is indicated by the occurrence of contorted, probable Paleozoic shale stratigraphically beneath Precambrian basement rock (Figure 3).

The VC-1 breccias are concentrated in two intervals. The deepest interval, between 844 and 856.1 m (Figure 3), includes a basal zone of contorted and fractured shale, an overlying tectonic breccia, and a molybdenite-bearing hydrothermal breccia. The upper breccia interval, spanning the depth range 826.3–835.4 m and including red beds of the Log Springs Formation (?), is a complex sequence believed to be tectonically and hydrothermally rebrecciated sedimentary breccia.

In addition to the disturbed Log Springs (?) interval, the upper breccia zone in VC-1 includes two heterolithologic breccias intersected in the intervals 831.3–832.7 and 834.0–835.4 m (Figure 3). These breccias, separated by brecciated limestone, contain approximately 50% (volume) angular to highly rounded clasts, up to at least 20 cm (average about 2 cm) in diameter, embedded in a chloritic to siliceous and calcareous, silty to sandy matrix which locally is turbulently flow foliated. The clasts comprise, in decreasing order of abundance, sandstone and siltstone, chert, massive fine-crystalline chlorite, partially dolomitized and mineralized limestone and limestone breccia (Figure 6), hydrothermal quartz crystal fragments and aggregates, and rare pyrite. The two breccias are separated by a 1.5 m-thick intercept of limestone breccia. This rock consists of mostly angular, subequant clasts of medium-crystalline calcite, averaging about 2 cm in diameter, embedded in a texturally and compositionally identical matrix.

These two breccia intervals and intervening brecciated limestone almost certainly had complex origins. We have tentatively identified the overlying chert-bearing hematitic breccia (Figure 3) as the Mississippian Log Springs Formation, probably a red soil or regolith developed on underlying carbonate strata. The subjacent breccias under discussion, then, could have formed initially by collapse during contemporaneous

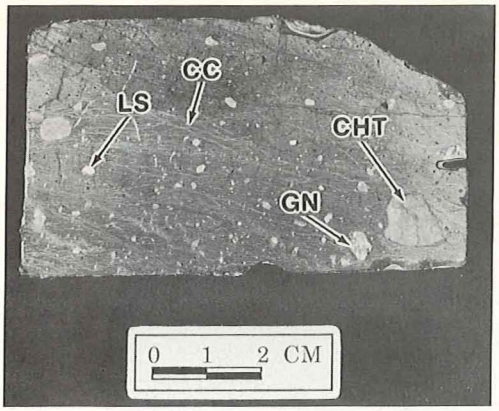

Fig. 7. Shaly, carbonate-rich, matrix-dominated tectonic breccia from the depth interval 850.4–850.5 m (top to left). CHT, recrystallized, sparsely chloritic chert clasts; GN, hydrothermally altered, phengite-rich clasts of Precambrian gneiss; and LS, recrystallized limestone clasts. Note anastamosing, late-stage, chlorite-calcite veinlets (CC).

solution activity in underlying Mississippian carbonates. However, mineralized Paleozoic carbonate clasts and delicate, angular hydrothermal quartz crystal fragments indicate that these breccias were probably modified well after the Paleozoic. There are no reported Paleozoic hydrothermal events in the Jemez Mountains [e.g., *Gardner et al.*, 1986].

Clast rounding and turbulent flow foliation in these breccias suggest that they were modified by hydrothermal fluidization. The porous, karstic network in which the breccias probably formed initially would provide excellent conduits for the escape of overpressured hydrothermal fluid. This fluid streaming would result in redistribution and alteration of original collapse debris.

Primary characteristics of the chert-bearing, brecciated red bed believed to be the Mississippian Log Springs Formation (Figures 3 and 5) were discussed in a previous section. A number of secondary features lead us to believe that this unit has also been rebrecciated. Both matrix and clasts show evidence of crushing and shearing (Figure 5), and slickensides are abundant. Clasts are commonly hydrothermally altered and mineralized; chert breccia clasts have been multiply rebrecciated and veined by quartz (Figure 5). The matrix of this red bed breccia also contains delicate, sharply faceted hydrothermal quartz crystal fragments, which could not have survived in their unabraded condition during normal sedimentary transport and deposition. All these features, taken together, lead us to believe that at the VC-1 site, the Log Springs Formation has been extensively disrupted by faulting along the Jemez fault zone.

By contrast with the breccias of the upper zone in VC-1, those of the lower zone, between 844 and 856.1 m (Figure 3), have unambiguous origins. The basal fractured shale and overlying, carbonate-rich breccia are clearly tectonic features. The overlying, molybdenite-bearing breccia was formed hydrothermally.

The contorted shale intersected at the base of the lower breccia zone, between depths of 852.6 and 856.1 m (Figure 3), is a quartz-illite rock with minor pyrite and chlorite. As in overlying sedimentary rocks, much of the layer silicate fraction is probably authigenic or diagenetic in origin. Both illite and chlorite, however, are extensively recrystallized, and illite microveinlets are locally common. This shale is thoroughly disrupted. Individual laminae can be traced only a few centimeters; slickensides and randomly oriented fractures are abundant. The shale is of unknown stratigraphic affiliation. However, since it was intersected beneath Precambrian gneiss, its present position in VC-1 must reflect postdepositional displacement. The gneiss most likely was moved above the shale by reverse or strike-slip faulting along the Jemez fault zone prior to late Miocene (the beginning of the current episode of normal displacement [*Aldrich and Laughlin*, 1984]). Alternatively, the gneiss could have been emplaced above the shale by gravity sliding.

Shaly, carbonate-rich, tectonic breccia overlies the basal shale and spans the interval 849.5–852.6 m (Figures 3 and 7). This breccia consists of 10–20% (volume) subrounded to angular clasts, averaging about 4 mm (up to 3 cm) in diameter, in a silty, argillaceous, commonly sheared and foliated matrix. The clasts comprise sandstone, siltstone, limestone, and chert as well as altered hydrothermal breccia and Precambrian gneiss (Figure 7) derived from immediately overlying units.

Intensely altered, molybdenite-bearing hydrothermal breccias were penetrated in VC-1 between depths of 844 and 849.5 m (Figure 3) immediately beneath similarly altered Precambrian gneiss. These breccias, distinctively bright gray-green in color due to phengitic alteration, consist of angular to highly rounded clasts, up to 5 (average about 1.5) cm in diameter, embedded in a locally flow-foliated rock-flour matrix (Figures 8 and 9). The clasts represent Precambrian orthogneiss, quartz-rich sandstone, polycrystalline hydrothermal vein quarts, and minor chert, as well as older breccias formed of one or more of these components. Relict sedimentary quartz grains in sandstone clasts commonly are surrounded by secondary quartz overgrowths, from which they are separated by rings of solid and fluid inclusions. The matrix of the breccia locally incorporates sand-size quartz clasts, probably derived in part by sandstone disaggregation.

Several textural features suggest that these breccias were developed by hydrothermal rather than tectonic processes. First, the general absence of slickensiding, shearing, and granulation strongly argues against their formation as fault breccias. Second, clasts commonly appear scalloped and abraded, and many are highly rounded (Figures 8 and 9), features which could indicate attrition during fluidization. Also, the matrix locally displays both lamellar and turbulent

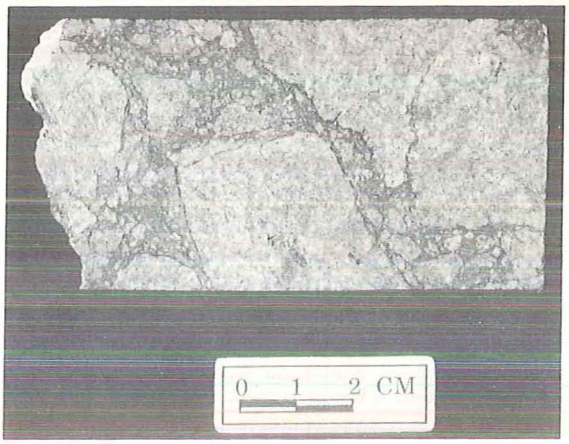

Fig. 8. Altered hydrothermal breccia from the depth interval 847.6–847.7 m (top to left). Clasts consist of quartz-sericitized gneiss and sandstone, rare chert, and older breccias incorporating one or more of these rock types. Dark matrix is rock flour altered to quartz, illite, phengite, and pyrite. Note flow-foliation in matrix, probably developed during fluidization.

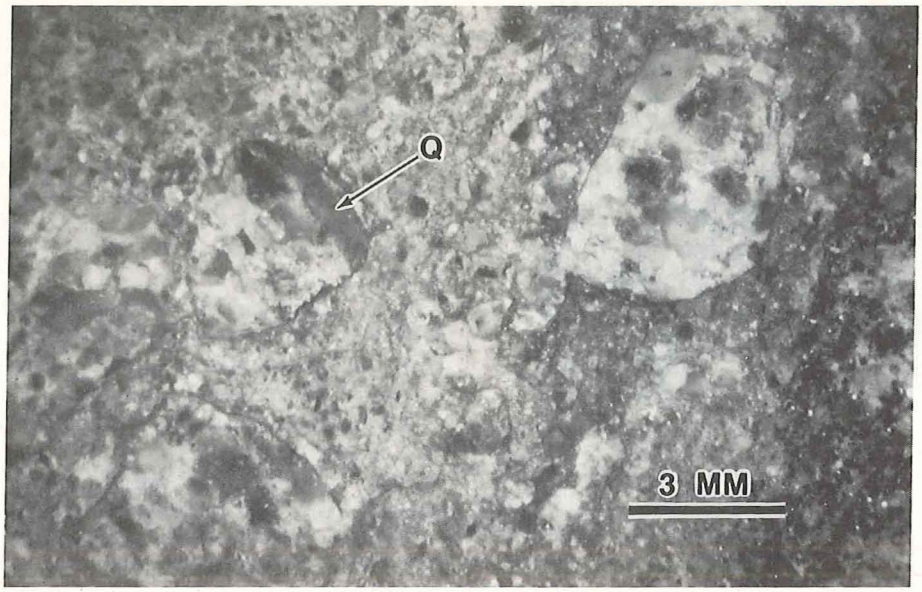

Fig. 9. Molybdenum-bearing hydrothermal breccia from a depth of 846.7 m, showing prominent flow-foliation in matrix. Also shown is a well-rounded clast of sandstone/gneiss breccia cut by a quartz (Q) microveinlet truncated at clast margins, attesting to formation of the veinlet prior to the most recent episode of hydrothermal brecciation. Molybdenite forms sparse, discontinuous microrims on several clasts but also occurs on late-stage fractures.

flow foliation (Figure 9), another feature indicative of hydrothermal fluid streaming.

HYDROTHERMAL ALTERATION

The entire prevolcanic sequence penetrated by VC-1 is both diagenetically and hydrothermally altered. Diagenesis and hydrothermal alteration of the Madera Limestone and Sandia Formation are detailed by *Keith* [this issue]. In this paper, we focus on alteration beneath the Sandia, principally in the complexly brecciated rocks described in the previous section.

The transition from dominantly diagenetic to principally hydrothermal regimes in the rocks penetrated by VC-1 coincides with the contact between the Pennsylvanian Sandia Formation and the Mississippian Log Springs Formation (?) at a depth of 826.3 m (Figure 3). Semiquantitative XRD analysis shows that the clay fraction above this contact is mostly mixed layer illite/smectite with subordinate chlorite. The illite/smectite is a highly ordered variety with 10–15% expandable (smectite) interlayers. Below the contact, illite with less than 5% expandable interlayers is the principal layer silicate. Numerous investigators [e.g., *Dunoyer de Segonzac*, 1970; *Środoń and Eberl*, 1984] have shown that the interlayer smectite content of illite/smectite diminishes as temperature is increased, either hydrothermally or diagenetically. The downward transition from illite/smectite in the Sandia shales to illite in the Log Springs (?) red beds, however, seems too abrupt to reflect simply a normal geothermal gradient in a deep sedimentary basin. There are at least two explanations for this sharp transition: tectonic disruption has juxtaposed formerly separate lower- and higher-grade diagenetic facies, or the interlayer smectite content of the illite/smectite in the brecciated Log Springs (?) Formation has decreased through interaction with high-temperature hydrothermal fluid.

The upper breccia interval (826.3–835.4 m; Figure 3) in VC-1 shows evidence of both prebreccia and postbreccia hydrothermal alteration. Clasts in this breccia zone are commonly altered and hydrothermally veined, with alteration textures and veinlets truncated at clast boundaries (Figure 5). The breccias also incorporate delicate hydrothermal quartz crystal fragments. The breccia intersected between depths of 831.3 and 832.7 m also hosts carbonate (limestone/dolomite) and carbonate breccia clasts which contain highly variable amounts of disseminated and veinlet magnetite, hematite, and pyrite. A few of these carbonate clasts also contain disaggregated, coarse-crystalline barite (Figure 6).

In addition to this prebreccia alteration, the rocks of the upper breccia interval in VC-1 are also sparsely cut by chlorite $\pm$ calcite microveinlets and very rarely by pyrite microveinlets; pyrite also locally replaces carbonate clasts. The breccia between 831.3 and 832.7 m is also cut by veinlets and irregular masses of chlorite with minor quartz and calcite. All three alteration minerals were probably formed during *Keith*'s [this issue] hydrothermal stage I, at temperatures of 200° $\pm$ 25°C.

Precambrian gneiss is among the most intensely altered rocks in VC-1. Original plagioclase in the gneiss is totally altered to fine-crystalline illite and phengite. Primary sphene and perhaps ilmenite are now mostly microcrystalline leucoxene. Biotite is replaced by iron-rich chlorite and may also be represented by disseminated muscovite. Primary magnetite is widely replaced by brick red hematite; apatite and zircon remain unaffected. The gneiss is also cut by numerous veinlets of quartz, quartz-sericite, quartz-phengite, and quartz-sericite-phengite, all of which commonly contain minor pyrite. The veinlets are multiply crosscutting (Figure 4). Quartz-sericite $\pm$ pyrite veinlets, the earliest formed, are cut by quartz-phengite $\pm$ sericite $\pm$ pyrite veinlets, which in turn are cut by quartz $\pm$ pyrite veinlets. The early veinlets may represent *Keith*'s [this issue] hydrothermal stage II, with an upper temperature limit, at this depth, of about 275°C. Subsequent veinlets in the gneiss probably formed during separate pulses of *Keith*'s [this issue] stage III alteration, which on the basis of phengite occurrence in other active hydrothermal systems, she suggests may have occurred at temperatures approaching 300°C. These results are consistent with paleotemperatures we have obtained from analysis of fluid inclusions in quartz veinlets cutting the gneiss and underlying hydrothermal breccia.

These hydrothermal breccias (844–849.5 m; Figure 3) are so intensely altered that no primary feldspar remains. Clasts and matrix are converted completely to quartz-illite-phengite-chlorite-pyrite aggregates locally incorporating minor calcite; primary quartz along with traces of apatite and zircon remains as relict phases. Phengite is much more abundant than in the overlying gneiss, imparting to the breccias a vivid gray-green coloration.

Hydrothermal veinlets are common in these breccias and, as in the overlying gneiss, comprise various combinations of quartz, illite, phengite, and pyrite; traces of chalcopyrite are locally present. Age relationships among veinlets are more ambiguous than in the gneiss, but in general, quartz-sericite veinlets are earliest and phengite-bearing veinlets are late stage. Many veinlets in clasts are abruptly cut off at clast margins (Figure 9), clearly indicating development prior to brecciation. Other veinlets, particularly those rich in quartz relative to illite and phengite, transect clasts and older matrix but abruptly terminate against younger matrix. We interpret this relationship to indicate formation of the veinlets between periods of brecciation.

Pyrite is the most abundant sulfide in these phengitic breccias, overall accounting for about 1% (weight) of the rock (Figure 3), but locally reaching concentrations of 3–5% in scattered 1- to 5-cm intervals. Pyrite deposition almost certainly accompanied each pulse of hydrothermal brecciation and alteration. The pyrite occurs principally as disseminated, generally subhedral grains and grain aggregates averaging about 1 mm (up to 3 mm) in diameter, but also in microveinlets with or without quartz, sericite, and phengite. The veinlet pyrite is accompanied by rare local traces of texturally similar but extremely fine-crystalline (<0.1 mm in diameter) chalcopyrite.

The breccias also locally host traces of molybdenite, which appears to have been the most recent sulfide deposited. Principally confined between depths of 845.8 and 847.5 m (Figure 3), the molybdenite occurs as thin, discontinuous films on phengite-coated fractures and on the surfaces of scattered clasts. We were unable to obtain enough of the molybdenite for complete characterization by XRD, but its identity was confirmed with the scanning electron microscope. The sulfide has the submetallic appearance and typical blue-gray sheen of the 2H polymorph, characteristic of Climax-type stockwork molybdenum deposits such as those of the nearby Questa caldera in northern New Mexico [*Leonardson et al.*, 1983].

At least five stages of alteration and mineralization in these hydrothermal breccias are suggested by crosscutting and replacement textures. During an early stage, corresponding in part to *Keith*'s [this issue] stage I, quartz-rich sandstone and Precambrian granitic gneiss were replaced by quartz + chlorite ± sericite and pyrite, then flooded (sandstone only) and veined with coarse, polycrystalline quartz, and finally tectonically or hydrothermally brecciated. The rock-flour matrix of the newly formed breccia was further altered to quartz and micaceous illite with minor pyrite (Keith's stage II?). This altered rock was hydrothermally rebrecciated, with attendant fluidization. The matrix and some clasts in this late breccia were replaced by quartz, illite, pyrite, and phengite during several pulses possibly representing *Keith*'s [this issue] alteration stage III. During each pulse, fractures in the breccia, at least partially hydraulic in origin, were filled by quartz veinlets also containing variable amounts of illite, phengite, and pyrite. Sparse molybdenite mineralization accompanied or shortly followed this late-stage phengitic alteration. The age of the molybdenite relative to late interbreccia quartz veinlets could not be determined.

Tectonic breccias intersected between 849.5 and 852.6 m are cut by numerous, anastamosing chlorite-calcite veinlets (Figures 3 and 7). These veinlets disrupt matrix and all clasts, including altered hydrothermal breccia and Precambrian gneiss from immediately overlying intervals. The veinlets may represent the most recent hydrothermal alteration of the deep VC-1 breccias.

FLUID INCLUSIONS

The hydrothermal breccias of VC-1 are riddled with small fluid inclusions, concentrated in quartz, that confirm the complex hydrothermal history suggested by alteration mineralogy and texture [see also *Sasada*, this issue]. As we will discuss in detail later in this section, the inclusions form distinct, low- and high-salinity compositional groups. Inclusions of both groups, however, are texturally identical and can be distinguished from each other only by heating and freezing experiments. The inclusions are principally secondary, occurring as planar aggregates and curviplanar "veils," which are randomly oriented and intersect to form weblike networks. Unambiguous primary inclusions are rare, of low salinity, and confined to interbreccia quartz veinlets. Microthermometric measurements of these primary inclusions are very similar to those for low-salinity secondary inclusions in quartz clasts. This relationship suggests that dilute primary and secondary inclusions could be in part coeval.

Secondary fluid inclusions in the VC-1 breccias are small, ranging from <0.2 to 11 μm in diameter but averaging less than 1 μm in diameter. Highly irregular inclusions are most abundant, particularly among those larger than 3 μm in diameter, but elongate and equant varieties, some partially bounded by negative crystal faces, are also common. Most secondary inclusions are two phase and liquid dominated at room temperature, with vapor bubbles estimated to account for 5–15 vol %. However, vapor-rich inclusions are also locally present. Many of these clearly reflect necking [*Roedder*, 1984], but others, particularly those concentrated with liquid-rich, low-salinity inclusions along single planes, appear to have undergone minimal modification since trapping. These coexisting liquid- and vapor-rich inclusions are believed to indicate boiling.

High- and low-salinity inclusions in the VC-1 breccias respond much differently to freezing procedures. High-salinity inclusions freeze abruptly upon supercooling at −65°C to −74°C, forming a dense, brownish, subtranslucent solid. They become conspicuously granular appearing, probably due to the onset of melting, at about −50°C, and show definite melting by −40°C. Low-salinity inclusions, by contrast, freeze upon supercooling at −40°C to −45°C without discoloration; melting commences at about −28°C.

The very low initial melting point of the high-salinity inclusions indicates that they contain appreciable calcium chloride or (much less likely) magnesium chloride in addition to sodium chloride [*Roedder*, 1984]. The initial −28°C melting temperature for the low-salinity inclusions indicates that they contain dominantly or exclusively sodium chloride waters.

Homogenization temperatures and corresponding ice-melting temperatures (freezing-point depressions) were measured for 55 two-phase, liquid-dominated fluid inclusions in two hydrothermal breccia samples (from depths of 846 and

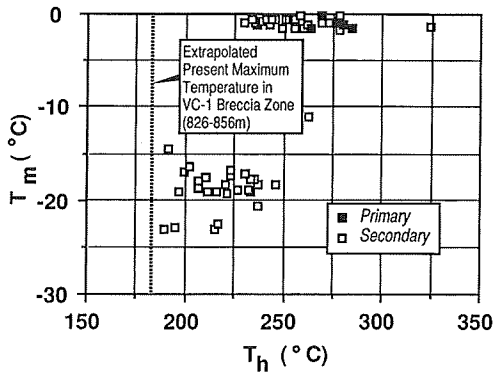

Fig. 10. Plot of homogenization temperatures versus ice-melting temperatures (freezing-point depressions) for 55 fluid inclusions in quartz from the hydraulically fractured and hydrothermally brecciated interval between depths of 842.9 and 847.7 m. The inclusions form two distinct compositional groups: one characterized by dilute, high-temperature fluids, the other by fluids of moderate temperature and high salinity.

846.7 m) and from hydraulically (?) fractured Precambrian gneiss at 842.9 m. Since ice-melting temperatures could be measured reliably in these samples only for inclusions larger than 2.5 μm in diameter, a bias in favor of larger inclusions could have been introduced. However, the distribution of homogenization temperatures for these larger inclusions is very similar to the temperature distribution for all inclusions regardless of size. This similarity suggests that the large inclusions are representative of those spanning the full size range.

The inclusions analyzed form distinct low- and high-salinity populations. These are clearly separated on a plot of homogenization temperatures versus corresponding ice-melting temperatures (Figure 10). All but two of the 17 high-salinity inclusions show ice-melting temperatures between -16.5°C and -23.1°C, and homogenize to the liquid phase at temperatures ranging from 189.4°C to 245.7°C. By contrast, 27 of 28 low-salinity inclusions, with ice-melting temperatures tightly confined between -0.1°C and -1.8°C, homogenize in a much higher temperature range between 229.5°C and 283.9°C. Geologic evidence to be discussed in the following section strongly suggests that inclusions of the low-salinity group were trapped at shallow depth. Measured homogenization temperatures for these inclusions therefore are probably very close to trapping temperatures. The trapping depth range for the high-salinity inclusions is unknown. In both cases, we believe that pressure corrections [*Potter*, 1977] are unwarranted.

Fluid-inclusion data obtained for VC-1 have been plotted on an enthalpy-chloride diagram (Figure 11), often used to assess the origins of deep geothermal waters [*Truesdell and Fournier*, 1976]. Fluids derived by boiling are represented on these diagrams as points along steam-loss lines radiating from the saturated steam point at 0% chloride and an enthalpy of 2775 kJ/kg at 284°C. A dilution line similarly emanates from the chloride-enthalpy point for cold water (in this case assumed to be Jemez River water) and constrains fluid compositions possible through mixing. Figure 11 demonstrates that the high- and low-salinity inclusion fluids in the VC-1 breccias could not have formed from one another through boiling or dilution. Compositional differences within groups, however, could be due in part to either or both processes, and to subtle changes in reservoir conditions during the evolution of multiple hydrothermal systems.

MODEL FOR HYDROTHERMAL BRECCIATION

The fluid-inclusion data discussed above can be combined with paragenetic information from alteration studies as well as the local geologic history to model hydrothermal brecciation at the VC-1 site. The model should have general application in similar settings elsewhere.

The following observations, presented in previous sections, are critical in formulating such a model. First, the VC-1 site is immediately adjacent to the Valles caldera complex, and thus to a potent magmatic heat source. Second, the breccias were formed in the Jemez fault zone. Third, rounding of clasts and flow-foliation of the matrix suggest that the breccias were emplaced or modified by hydrothermal fluidization. Finally, fluid inclusions preserve evidence of boiling.

The absolute age of the VC-1 hydrothermal breccias is uncertain, since the youngest clasts are Paleozoic sedimentary rocks. In view of the hydrothermal history of the Jemez Mountains and the location of VC-1, however, it is compelling to assume that these breccias are genetically related to the Valles caldera complex. Dated, post-Precambrian hydrothermal events in the Jemez Mountains are confined to the late Cenozoic [e.g., *Wronkiewicz et al.*, 1984; *Gardner et al.*, 1986], so the age of hydrothermal brecciation and alteration at the VC-1 site is probably similarly constrained. Although each of the numerous volcanic episodes in the Jemez Mountains since about 16 Ma must have been accompanied by hydrothermal activity, only in the Valles caldera complex and in the Bland mining district, over 16 km southeast of VC-1, is there obvious evidence of this activity. Epithermal precious metal mineralization dated at about 6 Ma [*Wronkiewicz et al.*, 1984] in the Bland district is accompanied by widespread propylitic and local argillic alteration, but hydrothermal breccias are apparently absent. By contrast, hydrothermal breccias appear to be widespread in the Valles caldera complex, occurring in each of the two Valles CSDP core holes completed to date, VC-1 and VC-2A (Figure 1) [*Hulen et al.*, 1987].

Genetically linking the VC-1 hydrothermal breccias with formation of the Valles caldera complex constrains not only their age, but also their depth of formation. The oldest deposits of the caldera complex, the Lower Tuffs of *Nielson and Hulen* [1984], are believed to range in age from 3.6 to 1.45 Ma [*Self et al.*, 1986]. However, the deep brecciation is much more likely to have accompanied (or followed) formation of the

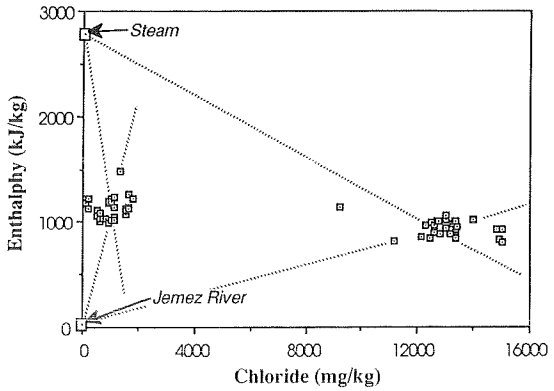

Fig. 11. Chloride-enthalpy diagram calculated from the fluid-inclusion data presented in Figure 10. Characteristics of Jemez River water from *Vuataz and Goff* [1986]. Diagram demonstrates that high- and low-salinity inclusion fluids in the VC-1 hydrothermal breccias could not have been derived from one another through either boiling or mixing.

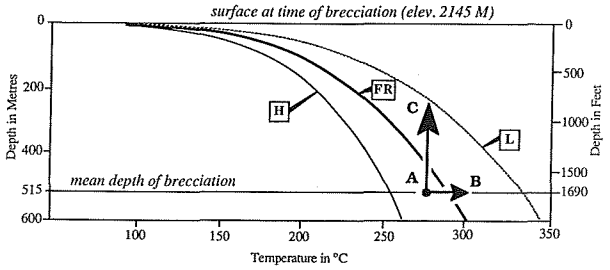

Fig. 12. Depth versus temperature plot and boiling point curves calculated for pure water and various relevant pressures at the time of hydrothermal brecciation at the VC-1 site. FR is the boiling point curve at pressures required to hydrofracture. H and L are hydrostatic and lithostatic boiling point curves, respectively, shown for comparison. Originating at the mean depth of brecciation, path AB symbolizes hydrofracturing due to increased heating. Path AC represents hydraulic rock rupture in response to rapid pressure release.

Valles caldera (1.12 Ma [*Self et al.*, 1986]) or its precursor, the Toledo caldera (1.45 Ma [*Self et al.*, 1986]). An upper age limit of brecciation is provided by the unaltered, postbreccia, 0.13- to 0.6-Ma rhyolitic volcanic sequence penetrated in the upper 333 m of VC-1 (Figure 2). Since this rhyolitic sequence had not yet been emplaced, the land surface at the time of brecciation would have been at an elevation of about 2145 m. (It is also assumed that the contemporaneous water table was at or near that paleosurface). Molybdenite-bearing hydrothermal breccias in VC-1 are presently situated between depths of 844.0 and 849.5 m (Figure 3). If they have not been displaced since formation, these breccias developed at an original mean depth of about 515 m.

Location of the breccias within a branch of the Jemez fault zone adjacent to the Valles caldera implies the state of stress at the time of brecciation. *Aldrich and Laughlin* [1984] have shown that the Jemez fault zone has undergone exclusively normal movement since 7–4 Ma, implying regional extension. Steep southeast dips measured along the Jemez fault zone [*Goff and Kron*, 1980] and on fractures in the VC-1 core demonstrate that this extension has taken place in a northwest-southeast direction, defining the least principal horizontal stress axis. Tectonism accompanying formation of the Valles caldera complex was also extensional [*Smith and Bailey*, 1968] in the shallow interval under discussion.

In an extensional tectonic environment, a rock will fail by hydraulic rupture when fluid pressure (P_{fr}) exceeds the least principal stress by an amount equal to the rock's tensile strength [*Hubbert and Willis*, 1957; *Phillips*, 1972; *Grindley and Browne*, 1976; *Fournier*, 1983]. *Hubbert and Willis* [1957] have shown that in such a regime, P_{fr} is approximately equal to one third the sum of the lithostatic load (S_z) and twice the hydrostatic fluid pressure (P_h):

$$P_{fr} \cong \frac{(S_z + 2P_h)}{3} \quad (1)$$

Assuming for the VC-1 site an average rock density of 2.7 g/cm^3 and hydrostatic pressures approximating those of the boiling point versus depth curve for pure water, then at the time and assumed depth of brecciation, S_z would have been about 13.7 MPa and P_h about 4.4 MPa. The corresponding theoretical pressure required to hydrofracture therefore would have been about 7.5 MPa, or 0.0146 MPa/m.

This theoretical P_{fr} is slightly less than the value predicted from rock breakdown pressures obtained during hydraulic fracturing experiments at the nearby Fenton Hill Hot Dry Rock site (Figure 1). *Murphy et al.* [1983] estimated from these experiments that an average fluid pressure of 75.04 MPa (0.0167 MPa/m) would be required to induce hydrofracturing at a depth of 4500 m. This corresponds to a P_{fr} value of 8.6 MPa at the assumed 515-m depth of brecciation of the VC-1 rocks. Since it is unclear to what extent the Jemez fault zone and the Fenton Hill site are structurally equivalent, we will use the lower, theoretical P_{fr} gradient (0.0146 MPa/m) in the breccia models which follow.

Pressure gradients corresponding to lithostatic, hydrostatic, and hydrofracturing pressures can be used with thermodynamic data from the steam tables of *Keenan et al.* [1978] to prepare a family of boiling point versus depth curves that graphically define the physical conditions of hydrothermal brecciation in the Jemez fault zone at the VC-1 site (Figure 12). All curves are adjusted for elevation of the land surface at the time of brecciation (about 2145 m) and assume water saturation up to that surface. Although technically valid only for pure water, these curves differ little from those appropriate for the dilute fluids believed responsible for the brecciation. Under hydrostatic conditions, fluid temperatures along the fault zone would have been limited by those defining curve H (Figure 12). However, if the fault was tectonically or hydrothermally sealed, fluid temperatures could have risen above those of curve H, approaching those where boiling is controlled by the strength of the rock. By the above analysis, these temperatures are defined by curve FR in Figure 12. Curve L (Figure 12) defines temperatures required to flash fluids under lithostatic load. This flashing would take place only in an environment where the lithostatic pressure was equivalent to the least principal stress.

There are two end-member paths which could have resulted in hydrothermal brecciation at the VC-1 site. Path AB represents hydrofracturing in response to a temperature increase. As the fluid is heated along this path, its vapor pressure eventually exceeds that required to hydrofracture, and the rock ruptures. Large overpressures are unlikely, since even small fracturing events will buffer pressures at those defined by curve FR. Hydraulic fracturing due to a sudden decrease in confining pressure is symbolized by path AC (Figure 12). Such a pressure release at the VC-1 site could have been effected by seismic cracking of a hydrothermally sealed portion of the Jemez fault zone. In this case, extreme fluid overpressures and violent rock disruption are much more likely than along path AB, since the drop in confining pressure can be large and instantaneous. Such overpressures may be responsible for the fluidized textures locally common in the hydrothermal breccias of VC-1. The fluids may even have vented to the surface, forming explosion craters such as those of the active geothermal systems at Yellowstone National Park [*Muffler et al.*, 1971] and Waiotapu, New Zealand [*Hedenquist and Henley*, 1985].

Discussion and Conclusions

The deep breccias of VC-1 have complex multiple origins, not surprising in view of the core hole's location in a long-active fault zone adjacent to a major caldera complex hosting high-temperature geothermal systems. Tectonic breccias of the Jemez fault zone have localized subsequent hydrothermal brecciation. The age of this brecciation must be inferred, but geologic evidence strongly suggests that rock rupture was in-

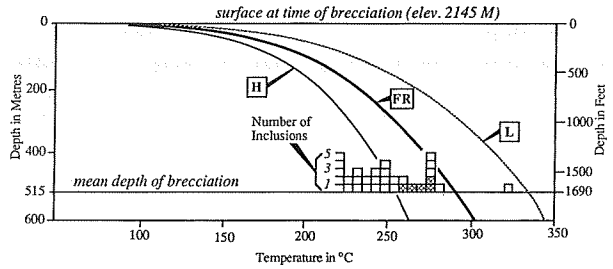

Fig. 13. Depth versus temperature plot and boiling point curves of Figure 12, showing homogenization temperatures for dilute, probable interbreccia fluid inclusions in the VC-1 hydrothermal breccias. Crosshatching indicates primary inclusions.

duced by hydrothermal fluid overpressuring accompanying formation of the late Cenozoic Valles caldera complex.

Fluid-inclusion characteristics, when studied in conjunction with alteration assemblages and textures as well as the local geologic history, can be used to deduce the mechanisms of hydrothermal brecciation. Homogenization temperatures for 13 of the 28 low-salinity fluid inclusions in the VC-1 hydrothermal breccias, when plotted at the assumed depth of brecciation, exceed temperatures defining the hydrostatic boiling point versus depth curve for pure water (curve H, Figure 13). This relationship supports the proposal that at the VC-1 site, the Jemez fault zone was hydrothermally sealed prior to each episode of hydrothermal brecciation, allowing pressures to approach those of curve FR. Hydrothermal brecciation was triggered through a rapid release in confining pressure or renewed heating. Boiling which produced and accompanied this brecciation is documented by coexisting, liquid- and vapor-rich, low-salinity fluid inclusions.

Once the boiling point was exceeded, flashing fluids in fractures and intergranular pores ruptured and comminuted enclosing rocks. In some cases, the resulting three-phase mixture (liquid + vapor + solid rock) was involved in fluidization, with further attrition of entrained rock particles. The increased surface area of these comminuted fragments facilitated hydrothermal alteration.

Homogenization temperatures of high-salinity fluid inclusions, when plotted at the same mean depth of brecciation at the VC-1 site (Figure 14), by contrast with those of coexisting dilute inclusions are well below temperatures defining a corresponding hydrostatic boiling point curve. This relationship clearly indicates that these saline fluids were not involved in the hydrothermal brecciation recorded by their younger, dilute counterparts.

The occurrence of molybdenite in the hydrothermal breccias of VC-1 further strengthens the hypothesis that these breccias are genetically related to the Valles caldera complex. The only other reported occurrence of this sulfide in the Jemez Mountains is in young (<1.12 Ma) intracaldera tuffs penetrated by CSDP core hole VC-2A, at Sulphur Springs in the Valles caldera (Figure 1) [*Hulen et al.*, 1987]. Molybdenite in the Sulphur Springs rocks, like that of VC-1, is intimately associated with hydrothermal brecciation and intense quartz-sericite alteration. Hydrothermal phengite, an uncommon layer silicate abundant in the VC-1 breccias, is also common in VC-2A.

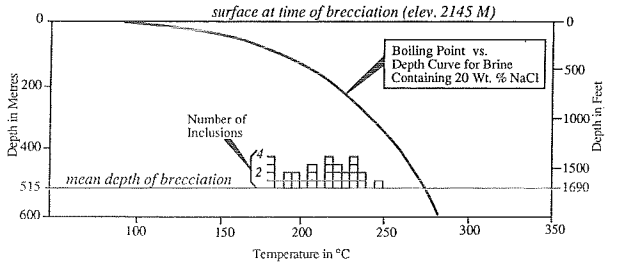

Fig. 14. Depth versus temperature plot and boiling point curve appropriate for fluid of 20% (weight) salinity [from *Haas*, 1971] under hydrostatic pressure at the time of brecciation at the VC-1 site, showing homogenization temperatures for high-salinity fluid inclusions in hydrothermal breccias.

The shallow molybdenum mineralization intersected in VC-2A is very similar to that occurring above some deeply concealed, Climax-type, stockwork molybdenite deposits [*Hulen et al.*, 1987]. The molybdenite, associated alteration, and hydrothermal brecciation encountered in VC-1 and VC-2A could represent high-level leakage from a deep, Climax-type hydrothermal system.

Our studies of the two Valles CSDP core holes have shown that, as in many New Zealand geothermal systems [*Grindley and Browne*, 1976; *Hedenquist and Henley*, 1985], hydrothermal brecciation has created or enhanced structural permeability in high-temperature geothermal systems of the Valles caldera. Discovery of these hydraulically fractured rocks, not recognized from previous studies based on rotary drill cuttings, exemplifies the value of continuous core from carefully monitored scientific drilling

Acknowledgments. This research was made possible by grant FE-FGO2-86ER13467.MOO1 from the Office of Basic Energy Sciences of the U.S. Department of Energy. Core photographs are the work of the Medical Illustrations Department of the University of Utah Medical Center. We thank M. C. Adams, F. Goff, T. E. C. Keith, and P. R. L. Browne for careful and extremely helpful reviews.

REFERENCES

Aldrich, M. J., and A. W. Laughlin, A model for the tectonic development of the southeastern Colorado Plateau boundary, *J. Geophys. Res.*, *89*, 10,207–10,218, 1984.

Armstrong, A. K., and B. L. Mamet, Biostratigraphy of the Arroyo Peñasco Group, Lower Carboniferous (Mississippian), north-central New Mexico, *Field Conf. Guideb. N. M. Geol. Soc.*, *25*, 145–158, 1974.

Baltz, E. H., and D. A. Myers, Porvenir Formation (new name)—And other revisions of nomenclature of Mississippian, Pennsylvanian, and Lower Permian rocks, southeastern Sangre de Cristo Mountains, New Mexico, *U.S. Geol. Surv. Bull.*, 1537-B, 39 pp., 1984.

Berger, B. R., Geologic-geochemical features of hot-spring precious metal deposits, Geologic characteristics of sediment- and volcanic-hosted disseminated gold deposits—Search for an occurrence model, *U.S. Geol. Surv. Bull.*, *1646*, 47–54, 1985.

Charles, R. W., R. J. Vidale-Buden, and F. Goff, An interpretation of the alteration assemblages at Sulphur Springs, Valles caldera, New Mexico, *J. Geophys. Res.*, *91*, 1887–1898, 1986.

Doell, R. R., G. B. Dalrymple, R. L. Smith, and R. A. Bailey, Paleomagnetism, potassium-argon ages, and geology of rhyolites and associated rocks of the Valles caldera, New Mexico, Studies in volcanology, *Mem. Geol. Soc. Am.*, *116*, 211–248, 1968.

DuChene, H. R., Pennsylvanian rocks of north-central New Mexico, *Field Conf. Guideb. N. M. Geol. Soc.*, *25*, 159–165, 1974.

Dunoyer de Segonzac, G., The transformation of clay minerals during diagenesis and low-grade metamorphism—A review, *Sedimentology*, *15*, 281–346, 1970.

Fournier, R. O., Active hydrothermal systems as analogues of fossil systems, The role of heat in the development of energy and mineral resources in the northern Basin and Range province, *Geotherm. Res. Counc. Spec. Rep.*, *13*, 263–284, 1983.

Gardner, J. N., F. Goff, S. Garcia, and R. C. Hagan, Stratigraphic relations and lithologic variations in the Jemez volcanic field, New Mexico, *J. Geophys. Res.*, *91*, 1763–1778, 1986.

Goff, F., and J. N. Gardner, Geologic map of the Sulphur Springs area, Valles caldera geothermal system, New Mexico, *Rep. LA-8634-MAP*, Los Alamos Natl. Lab., Los Alamos, N. M., 1980.

Goff, F., and A. Kron, In-progress geologic map of Cañon de San Diego, Jemez Springs, New Mexico, and lithologic log of Jemez Springs geothermal well, *Map LA-8276-MAP*, Los Alamos Sci. Lab., Los Alamos, N. M., 1980.

Gordon, C. H., Notes on the Pennsylvanian Formations in the Rio Grande Valley, New Mexico, *J. Geol., 15*, 805–816, 1907.

Grindley, G. W., and P. R. L. Browne, Structural and hydrologic factors controlling the permeabilities of some hot-water geothermal fields, paper presented at 2nd U. N. Symposium on Development and Use of Geothermal Resources, San Francisco, Calif., 1976.

Haas, J. L., The effect of salinity on the maximum thermal gradient of a hydrothermal system at hydrostatic pressure, *Econ. Geol., 66*, 940–946, 1971.

Hedenquist, J. W., and R. W. Henley, Hydrothermal eruptions in the Waiotapu geothermal system, New Zealand: Their origin, associated breccias, and relation to precious metal mineralization, *Econ. Geol., 80*, 1640–1668, 1985.

Heiken, G., F. Goff, J. Stix, S. Tamanyu, M. Shafiqullah, S. Garcia, and R. Hagan, Intracaldera volcanic activity, Toledo caldera and embayment, Jemez Mountains, New Mexico, *J. Geophys. Res., 91*, 1799–1815, 1986.

Hubbert, M. K., and D. G. Willis, Mechanics of hydraulic fracturing, *Trans. Inst. Min. Metall. Pet. Eng., 210*, 153–166, 1957.

Hulen, J. B., and D. L. Nielson, Stratigraphic permeability in the Baca geothermal system, Redondo Creek area, Valles caldera, New Mexico, *Geotherm. Res. Counc. Trans., 6*, 27–30, 1982.

Hulen, J. B., and D. L. Nielson, Hydrothermal alteration in the Baca geothermal system, Redondo dome, Valles caldera, New Mexico, *J. Geophys. Res., 91*, 1867–1886, 1986*a*.

Hulen, J. B., and D. L. Nielson, Stratigraphy and hydrothermal alteration in well Baca-8, Sulphur Springs area, Valles caldera, New Mexico, *Geotherm. Res. Counc. Trans., 10*, 187–192, 1986*b*.

Hulen, J. B., D. L. Nielson, F. Goff, J. N. Gardner, and R. W. Charles, Molybdenum mineralization in an active geothermal system, Valles caldera, New Mexico, *Geology, 15*, 748–752, 1987.

Izett, G. A., J. D. Obradovich, C. W. Naeser, and G. T. Cebula, Potassium-argon and fission-tract zircon ages of Cerro Toledo rhyolite tephra in the Jemez Mountains, New Mexico, *U.S. Geol. Surv. Prof. Pap.*, 1199-D, 37–43, 1980.

Keenan, J. H., F. G. Keyes, P. G. Hill, and J. G. Moore, *Steam Tables and Thermodynamic Properties of Water Including Vapor, Liquid, and Solid Phases*, 156 pp., John Wiley, New York, 1978.

Keith, T. E. C., Alteration in the Madera Limestone and Sandia Formation from core hole VC-1, Valles caldera, New Mexico, *J. Geophys. Res.*, this issue.

Kelley, V. C., and S. A. Northrop, Geology of Sandia Mountains and vicinity, New Mexico, *N. M. Bur. Mines Min. Res. Mem., 29*, 136 pp., 1975.

Laughlin, A. W., The geothermal system of the Jemez Mountains, New Mexico, and its exploration, in *Geothermal Systems—Principles and Case Histories*, edited by L. Rybach and L. J. P. Muffler, pp. 295–320, John Wiley, New York, 1981.

Lehrman, N. J., Geology and geochemistry of the McLaughlin hot-spring precious-metal deposit, California coast ranges, paper presented at Symposium on Bulk Mineable Precious Metal Deposits of the Western United States, Geol. Soc. of Nev., Sparks, Nev., 1987.

Leonardson, R. W., G. Dunlop, V. L. Starquist, G. Bratton, J. W. Meyer, L. W. Osborne, S. A. Atkin, P. A. Molling, R. F. Moore, and S. D. Olmore, Preliminary geology and molybdenum deposits at Questa, New Mexico, in *The Genesis of Rocky Mountain Ore Deposits—Changes With Time and Tectonics*, pp. 151–155, Denver Region Exploration Geologists Society, Golden, Colo., 1983.

Loughlin, G. H., and A. H. Koschmann, Geology and ore deposits of the Magdalena mining district, New Mexico, *U.S. Geol. Surv. Prof. Pap., 200*, 168 pp., 1942.

McCallum, M. E., Experimental evidence for fluidization processes in breccia pipe formation, *Econ. Geol., 80*, 1523–1543, 1985.

Muffler, L. J. P., D. E. White, and A. H. Truesdell, Hydrothermal explosion craters in Yellowstone National Park, *Geol. Soc. Am. Bull., 82*, 723–740, 1971.

Murphy, H., Z. Dash, and L. Aamodt, Variation of earth stresses with depth near the Valles caldera, New Mexico, *Los Alamos Natl. Lab. Rep., ESS-4/83:461*, 27 pp., 1983.

Nielson, D. L., and J. B. Hulen, Internal geology and evolution of the Redondo Dome, Valles caldera, New Mexico, *J. Geophys. Res., 89*, 8695–8712, 1984.

Phillips, W. J., Hydraulic fracturing and mineralization, *J. Geol. Soc. London, 128*, 337–359, 1972.

Potter, R. W., Pressure corrections for fluid-inclusion homogenization temperatures based on the volumetric properties of the system $NaCl\text{-}H_2O$, *J. Res. U.S. Geol. Surv., 5*, 603–607, 1977.

Reynolds, D. L., Fluidization as a geological process, and its bearing on the problem of intrusive granites, *Am. J. Sci., 252*, 557–613, 1954.

Reynolds, R. C., Interstratified clay minerals, in *Crystal Structures of Clay Minerals and Their X-Ray Identification, Monogr. 5*, pp. 249–304, Mineralogical Society, London, 1980.

Roedder, E., Fluid inclusions, *Rev. Mineral., 12*, 644 pp., 1984.

Sasada, M., Microthermometry of fluid inclusions from the VC-1 core hole in Valles caldera, Mew Mexico, *J. Geophys. Res.*, this issue.

Self, S., F. Goff, J. N. Gardner, J. F. Wright, and W. M. Kite, Explosive rhyolitic volcanism in the Jemez Mountains—Vent locations, caldera development, and relation to regional structure, *J. Geophys. Res., 91*, 1779–1798, 1986.

Shevenell, L., F. Goff, F. Vuataz, R. Trujillo, D. Counce, C. Janík, and W. Evans, Hydrochemical data for thermal and nonthermal waters and gases of the Valles caldera–southern Jemez Mountains region, New Mexico, *Los Alamos Natl. Lab. Rep., La-10923-OBES*, 100 pp., 1987.

Sibson, R. H., Fault rocks and fault mechanisms, *J. Geol. Soc. London., 133*, 191–213, 1977.

Siemers, W. T., The Pennsylvanian System, Socorro region, New Mexico—Stratigraphy, petrology, depositional environments, *Field Conf. Guideb. N. M. Geol. Soc., 34*, 147–155, 1983.

Sillitoe, R. H., Ore-related breccias in volcanoplutonic arcs, *Econ. Geol., 80*, 1467–1514, 1985.

Smith R. L., and R. A. Bailey, Resurgent cauldrons, Studies in Volcanology, edited by R. R. Coats, R. L. Hay, and C. A. Anderson *Mem. Geol. Soc. Am., 116*, 613–632, 1968.

Środoń, J., Precise identification of illite/smectite interstratifications by X-ray diffraction, *Clays Clay Miner., 28*, 401–411, 1980.

Środoń, J., and D. D. Eberl, Illite, *Rev. Mineral., 13*, 495–544, 1984.

Truesdell, A. H., and R. O. Fournier, Calculation of deep temperatures in geothermal systems from the chemistry of boiling spring waters of mixed origin, paper presented at 2nd U. N. Symposium on Development and Use of Geothermal Resources, San Francisco, Calif., 1976.

Truesdell, A. H., and C. J. Janik, Reservoir processes and fluid origins in the Baca geothermal system, Valles caldera, New Mexico, *J. Geophys. Res., 91*, 1817–1833, 1986.

Union Oil Company of California, Baca project, geothermal demonstration power plant, final report, cooperative agreement ET-78-F-03-1717, 436 pp., Santa Rosa, Calif., 1982.

Vuataz, F. D., and F. Goff, Isotope geochemistry of thermal and nonthermal waters in the Valles caldera, Jemez Mountains, northern New Mexico, *J. Geophys. Res., 91*, 1835–1853, 1986.

White, A. F., Chemical and isotopic characteristics of fluids within the Baca geothermal reservoir, Valles caldera, New Mexico, *J. Geophys. Res., 91*, 1855–1866, 1986.

Wronkiewicz, D., D. Norman, G. Parkison, and K. Emanuel, Geology of the Cochiti mining district, Sandoval County, New Mexico, *Field Conf. Guideb. N. M. Geol. Soc., 35*, 219–222, 1984.

J. B. Hulen and D. L. Nielson, University of Utah Research Institute, Earth Science Laboratory, 391 Chipeta Way, Suite C, Salt Lake City, UT 84108.

(Received March 31, 1987;
revised August 14, 1987;
accepted September 3, 1987.)